



Exploring pore-scale production characteristics of oil shale after CO₂ huff 'n' puff in fractured shale with varied permeability

Tianhan Xu¹ · Jian Wang¹ · Yuhao Lu¹ · Danling Wang³ · Li Yu⁴ · Ye Tian^{1,2}

Received: 30 April 2023 / Revised: 25 July 2023 / Accepted: 22 January 2024
© The Author(s) 2024

Abstract

Recent studies have indicated that the injection of carbon dioxide (CO₂) can lead to increased oil recovery in fractured shale reservoirs following natural depletion. Despite advancements in understanding mass exchange processes in subsurface formations, there remains a knowledge gap concerning the disparities in these processes between the matrix and fractures at the pore scale in formations with varying permeability. This study aims to experimentally investigate the CO₂ diffusion behaviors and in situ oil recovery through a CO₂ huff 'n' puff process in the Jimsar shale oil reservoir. To achieve this, we designed three matrix–fracture models with different permeabilities (0.074 mD, 0.170 mD, and 0.466 mD) and experimented at 30 MPa and 91 °C. The oil concentration in both the matrix and fracture was monitored using a low-field nuclear magnetic resonance (LF-NMR) technique to quantify in situ oil recovery and elucidate mass-exchange behaviors. The results showed that after three cycles of CO₂ huff 'n' puff, the total recovery degree increased from 30.28% to 34.95% as the matrix permeability of the core samples increased from 0.074 to 0.466 mD, indicating a positive correlation between CO₂ extraction efficiency and matrix permeability. Under similar fracture conditions, the increase in matrix permeability further promoted CO₂ extraction efficiency during CO₂ huff 'n' puff. Specifically, the increase in matrix permeability of the core had the greatest effect on the extraction of the first-cycle injection in large pores, which increased from 16.42% to 36.64%. The findings from our research provide valuable insights into the CO₂ huff 'n' puff effects in different pore sizes following fracturing under varying permeability conditions, shedding light on the mechanisms of CO₂-enhanced oil recovery in fractured shale oil reservoirs.

Keywords Shale reservoir · Hydraulic fracturing · CO₂ huff 'n' puff · NMR · Production characteristics

1 Introduction

The continuous advancement of exploration and development technology has made shale oil a focal point for oil and gas exploration in several countries worldwide (Sharma

et al. 2020; Taheri-Shakib and Kantzas 2021; Li et al. 2023). Despite the presence of oil in shale rocks, they are unable to flow into wellbores at profitable rates. The current method of utilizing massive hydraulic fracturing and long horizontal wells has a crude oil recovery rate of less than 10%. Additionally, the production rate experiences a rapid decline within the first 1–2 years, particularly in the targeted reservoirs of these developments, due to their extremely low permeability. In light of these challenges, implementing enhanced oil recovery (EOR) techniques is crucial to boost production and enhance profitability. Recent reports suggest that the huff 'n' puff method, utilizing CO₂ or N₂, shows promise for enhanced oil recovery (EOR) in shale oil reservoirs (Enab and Emami-Meybodi 2021; Mahzari et al. 2021; Liu et al. 2023). Su et al. (2022) proposed that the injection of CO₂ for EOR not only significantly improves the recovery efficiency of shale reservoirs but also enables the sequestration of CO₂ within the reservoir, thereby supporting the achievement of the carbon peaking and carbon neutrality

✉ Jian Wang
199331010008@swpu.edu.cn

✉ Ye Tian
ytian@swpu.edu.cn

¹ State Key Laboratory of Oil and Gas Reservoir Geology and Exploitation, Southwest Petroleum University, Chengdu 610500, Sichuan, China

² Institute for Carbon Neutrality, Southwest Petroleum University, Chengdu 610500, Sichuan, China

³ Research Institute of Shenzhen Branch of CNOOC (China) Co., Ltd, Shenzhen 518000, Guangdong, China

⁴ PetroChina Huabei Oilfield Company, Cangzhou 062552, Hebei, China

goals and facilitating the implementation of carbon capture, utilization, and storage (CCUS) strategies.

It is widely assumed that CO₂ can enter the shale matrix and mobilize local oil. Gas diffusion, low interfacial tension, and light hydrocarbon extraction are the primary CO₂ EOR mechanisms (Burrows et al. 2020; Menefee and Ellis 2020; Chaturvedi and Sharma 2022). Some scholars have examined the effectiveness of utilizing shale reservoirs with different pore scales (Wei et al. 2020). However, there is still a lack of research on the mechanism of CO₂ adsorption and mass exchange as well as the reservoir reforming mechanism in shale reservoirs with different permeability.

Fractures found within the rock matrix have the potential to enhance hydrocarbon deliverability and increase drainage area, leading to improved oil production. In the case of tight matrix-fracture systems, a CO₂ exposure experiment conducted by Wang et al. (2020) using Qianjiang basin shale rocks revealed that the conceptual CO₂ EOR mechanisms included oil swelling, viscosity reduction, and pressure and concentration driving. These effects played a crucial role in transporting the matrix oil to the fractures and ultimately to the producers.

NMR is useful for determining fluid content, rock/fluid interactions, and pore size distribution (Amer et al. 2022; Shen et al. 2022; Hu et al. 2023). For example, Liu et al. (2020) used low-field nuclear magnetic resonance (LF-NMR) to investigate the pore structure of upper cretaceous oil shales, revealing different pore types and variable connectivity between pores in the shale based on three T₂ distribution morphologies. Saeed et al. (2022) used LF-NMR to examine the variation of organic matter in the core, as well as the hydrothermal treatment pore size and porosity changes; Wang et al. (2017) investigated the mechanisms of oil mobilization in ordos basin rocks exposed to CO₂ under immiscible conditions using NMR T₂. As a result, they concluded that performing NMR tests under reservoir conditions is critical. Similarly, Wei et al. (2020) demonstrated CO₂ diffusion and production mechanisms by performing CO₂ injection in fractured chalk plugs using the LF-NMR technique.

Notably, the above papers did not address the CO₂ huff 'n' puff efficiency and mass transfer mechanisms in formations

characterized by varying degrees of permeability. This knowledge gap is a critical obstacle for field decision-making about construction feasibility, as it precludes a comprehensive understanding of the factors that influence the potential success of CO₂ storage in such settings.

We conducted a CO₂ huff 'n' puff experiment in 3 matrix-fracture models under reservoir conditions (91 °C and 30 MPa). This experiment employed LF-NMR to monitor the entire experimental process, to elucidate the adaptability of CO₂ huff 'n' puff in shale formations with varying permeabilities, as well as the primary recovery mechanism differences of pores at different scales during the process. The findings from our research serve a valuable complementary information regarding the CO₂ huff 'n' puff effects in different pore sizes following fracturing under varying permeability conditions, shedding light on the mechanisms of CO₂-enhanced oil recovery (EOR) in fractured shale oil reservoirs.

2 Materials and methods

2.1 Materials

2.1.1 Experimental cores

The shale cores used in the experiments were obtained from the lower sweet spot of the Lucaogou Formation shale oil reservoir. Pairs of cores with similar porosity and permeability were combined to form two groups, each consisting of two cores. The basic parameters of these cores are presented in Table 1. As shown in Table 1, cores #1 and #2 exhibited the highest permeability, whereas cores #3 and #4 had the lowest permeability.

To simulate the seepage characteristics of the CO₂–oil system between fractures and the matrix, in this study artificially fractured natural cores were used to conduct CO₂ huff 'n' puff mass transfer experiments. The cores were taken from the Lucaogou Formation in the Jimusar shale reservoir. The cores were first cut in half along the midline and were then filled with quartz sand to simulate post-fracturing

Table 1 Parameters of cores used in CO₂ huff 'n' puff experiments

Core number	Length (cm)	Diameter (cm)	Porosity (%)	Permeability (gas test) (10 ⁻³ μm ²)	Permeability after artificial fracturing (water test) (10 ⁻³ μm ²)
Core #1	6.82	2.50	9.58	0.074	91.16
Core #2	6.51	2.50	9.73	0.170	97.39
Core #3	6.57	2.50	9.15	0.466	90.54

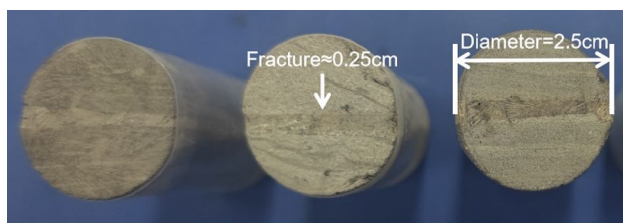


Fig. 1 Matrix/fracture model designed in this work. The two core halves were wrapped with a heat-shrink tube to maintain the fracture size

fractures. Heat-shrinkable tubing was used for fixing to ensure the overall strength of the cores and maintain the fracture size. The preparation process is illustrated in Fig. 1.

Due to our previous research, we have confirmed that CO₂ huff-n-puff can cause dissolution of mineral components within the core (Xu et al. 2022) and that the permeability of fractures may change during the CO₂ huff-n-puff process (Tan et al. 2023). To investigate further, we conducted permeability damage tests on cores from the same batch as this experiment. The results indicated that three cycles of CO₂ huff-n-puff resulted in permeability damage of around 10%, which would not significantly affect this experiment.

2.1.2 Experimental fluids

The physical and chemical properties of the dead oil used in this work are listed in Table 2. The chemical composition of this shale oil was analyzed using a THERMOFISHER®

Table 2 Physical and chemical properties of the used shale oil

Properties of the shale oil	Value
Viscosity at 91 °C (mPa s)	11.35
Density at 91 °C (kg/m ³)	0.887
Molecular weight (VPO)	222.3
Saturates content (wt%)	43.72
Aromatics (wt%)	26.59
Resin (wt%)	24.57
Asphaltenes (wt%)	5.12

Table 3 Composition of the shale oil

Carbon number	Content (wt%)	Carbon number	Content (wt%)	Carbon number	Content (wt%)
C ₉	0.94	C ₁₅	39.92	C ₂₁	6.53
C ₁₀	2.83	C ₁₆	12.11	C ₂₂	0.62
C ₁₁	3.21	C ₁₇	5.16	C ₂₃	0.60
C ₁₂	2.22	C ₁₈	0.62	C ₂₄₊	3.18
C ₁₃	8.95	C ₁₉	2.93		
C ₁₄	3.85	C ₂₀	6.33		

gas-chromatograph (GC)/mass spectrometer (MS), as illustrated in Table 3. Figure 2 presents the GC/MS spectrum of this oil. Because fractured core models cannot be completely saturated with live oil, the shale oil used in this study was dead oil with carbon numbers ranging from C₈ to C₂₄. The shale oil/CO₂ system's minimum miscibility pressure (MMP) was estimated to be 23.84 MPa using the slim tube method.

2.2 Methods

Figure 3 shows the simplified NMR experimental setup for CO₂ huff 'n' puff. A low-field NMR analysis system (MacroMR12-150H-I, Niumag®) was used in this study to perform online measurements of NMR T₂ spectrum, and NMR imaging. The magnetic flux density of the NMR scanner was 0.3 ± 0.05 T, and the pulse frequency range was 2–30 MHz.

The procedure of the CO₂ huff 'n' puff and NMR experiments was as follows: (1) All the shale cores were repeatedly washed with toluene, and heated in an oven at 100 °C for 24 h. (2) The cores were saturated with D₂O, and NMR scanning was performed on the cores after saturation with D₂O. The cores were then fully saturated with shale oil and aged at constant pressure for 5 days at 30 MPa. (3) The shale cores were taken out after depressurization and put into a heat-shrinkable casing. The cores were then sealed in the casing, and NMR scanning was performed on the oil-saturated cores. (4) The shale cores were put into the holder, and confining pressure was applied. The outlet end of the holder was then closed, and CO₂ was injected into the core at a constant rate of 0.5 mL/min from the inlet end. When the injection volume reached 0.5 times the pore volume, the injection of CO₂ was stopped, the valve was closed, and the holder was kept sealed for 10 h. (5) The injection end of the holder was opened, and depletion development was carried out with a constant decreasing pressure gradient until the pressure fell to 0.1 MPa. The volume of produced oil and gas was recorded, and NMR scanning was performed on the core after the huff 'n' puff process. The first cycle of huff 'n' puff was thus completed. Then steps (3) and (4) were repeated to start the next cycle of huff 'n' puff, with a total of three cycles.

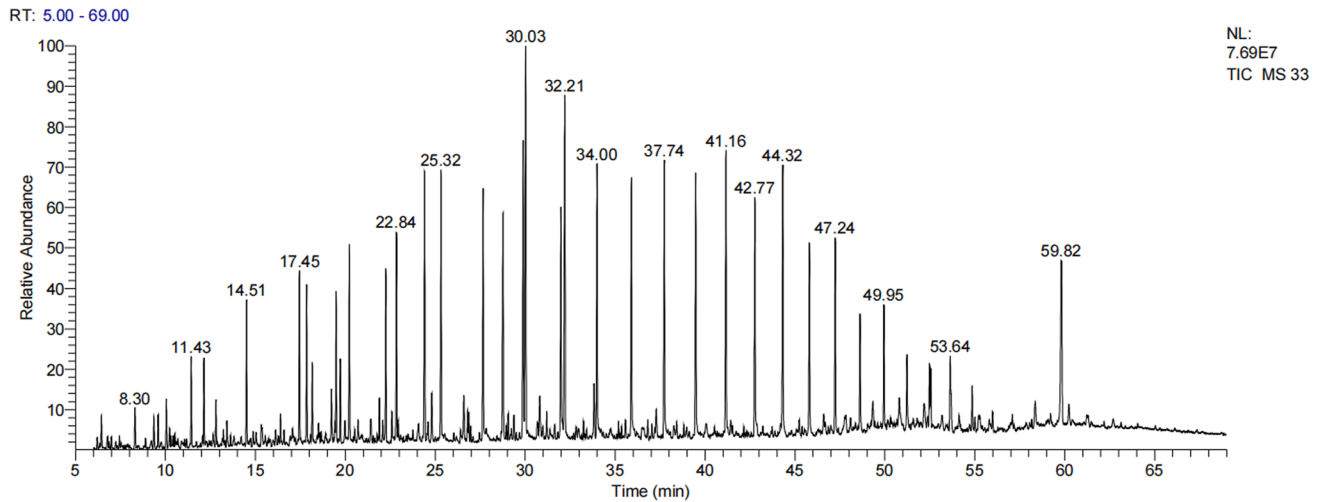


Fig. 2 GC/MS spectrum of the shale oil

The NMR transverse relaxation time (T_2) of a fluid in a pore is given by the following equation:

$$\frac{1}{T_2} = \frac{1}{T_{2,\text{bulk}}} + \frac{1}{T_{2,\text{surface}}} + \frac{1}{T_{2,\text{diffusion}}} \quad (1)$$

where $T_{2,\text{bulk}}$ is the bulk relaxation time of the pore-filling fluid (ms), $T_{2,\text{surface}}$ denotes the surface relaxation time (ms), and $T_{2,\text{diffusion}}$ represents the relaxation time induced by diffusion (ms). For fluid flow in porous media, $T_{2,\text{bulk}}$ is commonly neglected because the amplitude of $T_{2,\text{bulk}}$ is notably larger than that of T_2 and $T_{2,\text{diffusion}}$ is also neglected when the magnetic field used is uniform with a quite small field gradient. Hence, T_2 is primarily dependent on $T_{2,\text{surface}}$, which is related to the specific surface area of a pore. $T_{2,\text{surface}}$ can be expressed as (Yang et al. 2022)

$$\frac{1}{T_{2,\text{surface}}} = \rho \left(\frac{S}{V} \right)_{\text{pore}} \quad (2)$$

where ρ is the surface relaxivity ($\mu\text{m/ms}$), S is the interstitial surface area (μm^2), and V is the pore volume (PV), in μm^3 . S/V can be rewritten as a function of the dimensionless shape factor of a pore, F_s , and pore radius, r (μm)

$$\frac{S}{V} = \frac{F_s}{r} \quad (3)$$

Combing Eqs. (2) and (3), $T_{2,\text{the surface}}$ can be expressed as

$$T_{2,\text{surface}} = \frac{1}{\rho F_s} r \quad (4)$$

Fig. 3 Sketch of CO₂ huff 'n' puff experiment

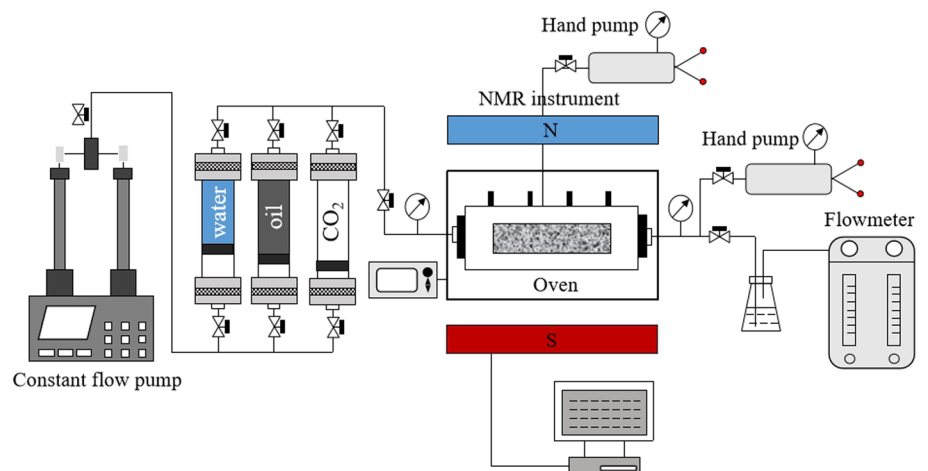


Fig. 4 T_2 spectrum distribution for saturated oil and after each cycle of huff 'n' puff

Its surface relaxivity and shape factor (F_s) can be presumed constant for a specific core. Consequently,

$$T_2 = Cr \tag{5}$$

where $C = 1/(\rho_s F_s)$ and is a constant conversion coefficient (ms/ μm).

To further quantitatively evaluate the degree of mobilization of shale oil in the matrix, the shale oil recovery degree of different pores before and after huff 'n' puff was calculated based on the characteristic that the sum of the intensities of the signals corresponding to a certain range of pore sizes after saturation of the core with oil is proportional to the amount of oil in the corresponding pore spaces (Zhao et al. 2022).

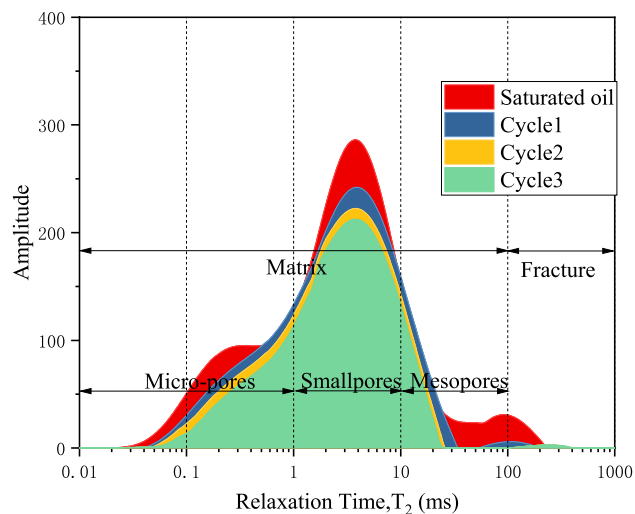
$$E_R = \frac{\sum_{T_{\min}}^{T_{\max}} W_0 - \sum_{T_{\min}}^{T_{\max}} W_h}{\sum_{T_{\min}}^{T_{\max}} W_0} \times 100\% \tag{6}$$

In Eq. (6), E_R is oil recovery degree of pores; T_{\min} is minimum relaxation time corresponding to a certain pore size in the T_2 spectrum distribution (ms); T_{\max} is maximum relaxation time corresponding to a certain pore size in the T_2 spectrum distribution (ms); W_0 is signal intensity of the T_2 spectrum in the initial state of saturation with oil; W_h is signal intensity of the T_2 spectrum after a certain cycle of huff 'n' puff.

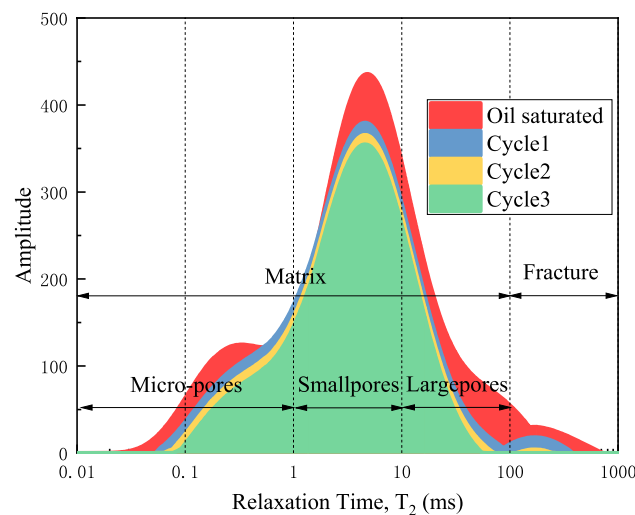
3 Results and discussion

3.1 T_2 spectrum distribution feature analysis

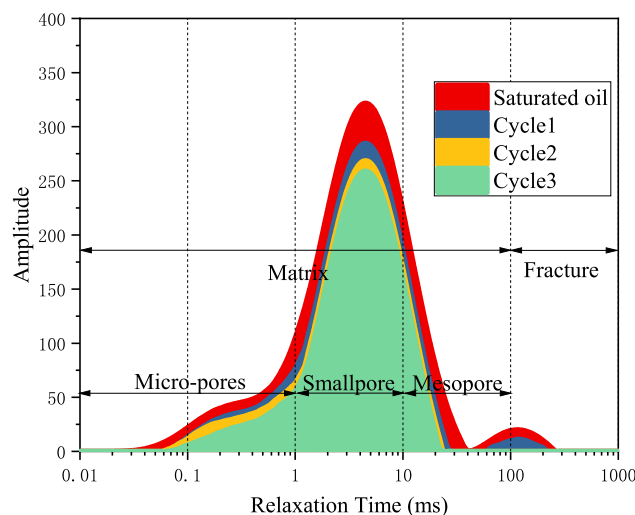
The NMR transverse relaxation time (T_2) distribution of the core was measured at different stages and is depicted in Fig. 4. Based on the principle that the T_2 relaxation time generated by shale oil in pores with varying pore sizes is proportional to the pore radius (Yang et al. 2013), the matrix and fractures in a core can be identified by examining the relaxation times corresponding to the peaks and troughs in the T_2 spectrum curve. Specifically, the matrix is represented by the corresponding interval when $0.1 \text{ ms} < T_2 < 100 \text{ ms}$, whereas fractures are represented when $100 \text{ ms} < T_2 < 1000 \text{ ms}$ (Al-Yaseri et al. 2015; Bardenhagen et al. 2014; De Boever et al. 2016), as shown in Fig. 4. To enable the analysis of shale oil production characteristics across pores with different sizes, matrix pore sizes were further classified into three categories, namely, micropores ($0.1 \text{ ms} < T_2 < 1 \text{ ms}$), small pores ($1 \text{ ms} < T_2 < 10 \text{ ms}$), and large pores ($10 \text{ ms} < T_2 < 100 \text{ ms}$)



(a)Core#1



(b)Core#2



(c)Core#3

(Chi and Heidari 2015; Liu et al.2021). The present study involves three huff ‘n’ puff cycles conducted on two sets of cores, each comprising three stages: CO₂ injection, soaking, and depressurization. The oil production during each cycle is distinctly visible in Fig. 4 (area difference between two cycles’ curves), which also allows for its calculation using Eqs. 6.

In Fig. 4, all three core samples display a significant decrease in NMR T_2 amplitude in the fracture and large pores interval, while the interval of micropores and small pores shows little variation. This observation is consistent with the early work reported by Wei et al. (2019) and indicates that, due to their better permeability, the oil in the fractures is produced first, followed by the gradual production of oil in the matrix in the order of large pores to small pores, as a result of CO₂ diffusion.

3.2 Analysis of matrix and fracture recovery degree

To validate the observed results, the total, matrix, and fracture recovery degree after each cycle of huff ‘n’ puff were calculated for three different permeability cores based on Eq. (6), as illustrated in Fig. 5. The data points represent the oil recovery at the end of each cycle, while the time scale denotes the duration of the experiment. It is observed that the cumulative oil recovery rapidly increases with increasing cycle number (time), and tends to plateau after the second cycle.

The recovery degree of fracture intervals in the three cores, as shown in Fig. 5c, are 84.48%, 99.96%, and 99.87%, respectively, which are much higher than those in the matrix interval, consistent with the observation results. However, due to the small proportion of fractures in the core, the main production of shale oil still occurs in the matrix interval. This also explains why the trends in Figs. 5a and b are basically the same. Figure 5b shows that for this fracture model, the recovery degree of the rock core matrix, i.e., the diffusion effect of CO₂, is positively correlated with the permeability of the rock core matrix. The higher the permeability of the core, the lower the resistance of the diffusion channels, and the stronger the ability of CO₂ to enter the matrix. Additionally, during the diffusion process of CO₂, the kinetic losses due to collisions between CO₂ molecules and pore wall surfaces are lower, resulting in better diffusion efficiency.

3.3 Analysis of shale oil recovery degree in different core permeabilities

The shale oil recovery degree determined by the NMR T_2 parameter for three pore intervals is plotted in Fig. 6. It is

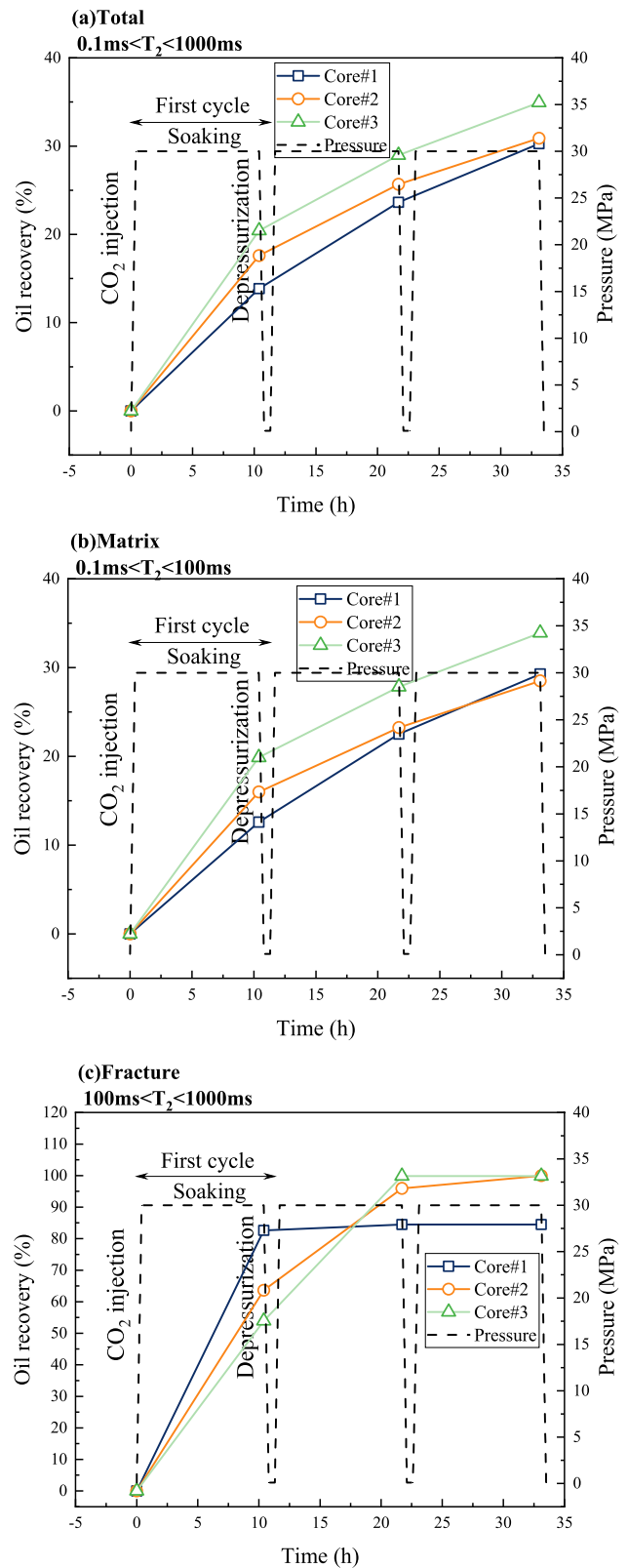


Fig. 5 Oil-recovery profiles of CO₂ huff ‘n’ puff plotted against cycle numbers (time) in matrix and fracture

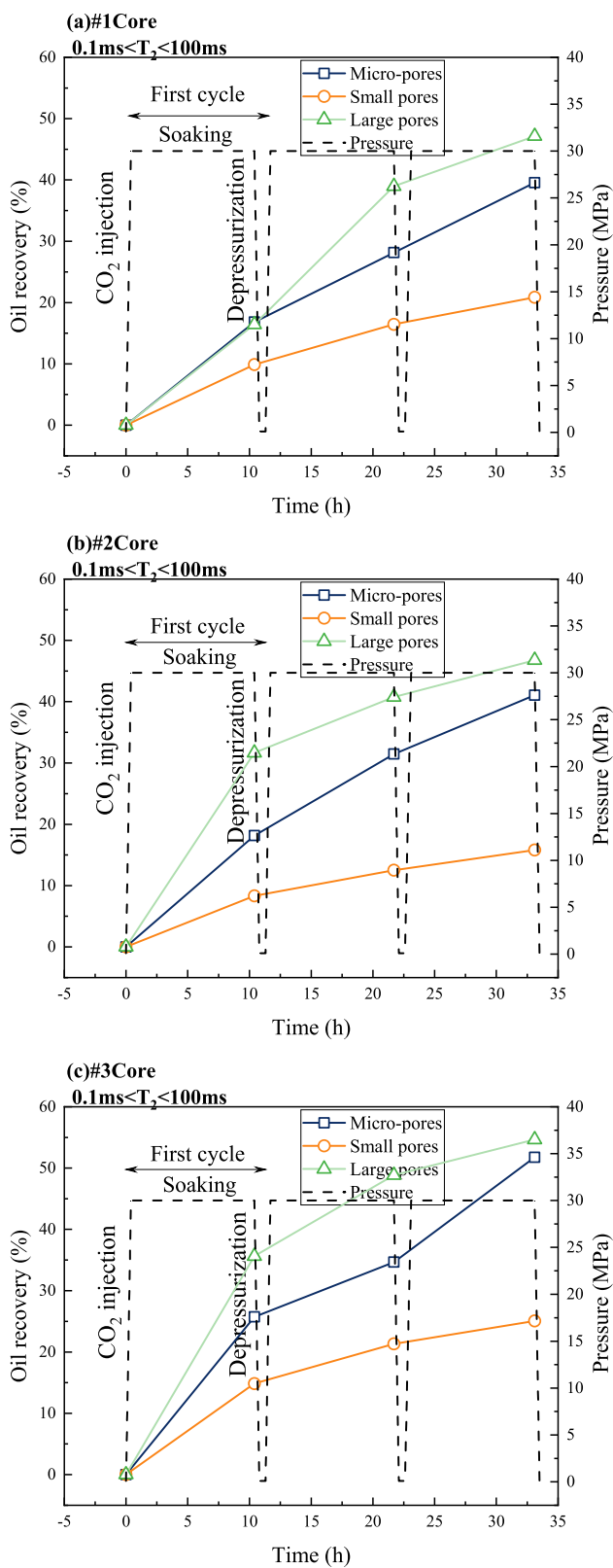


Fig. 6 Oil-recovery profiles of CO₂ huff 'n' puff plotted against cycle numbers (time) in different cores

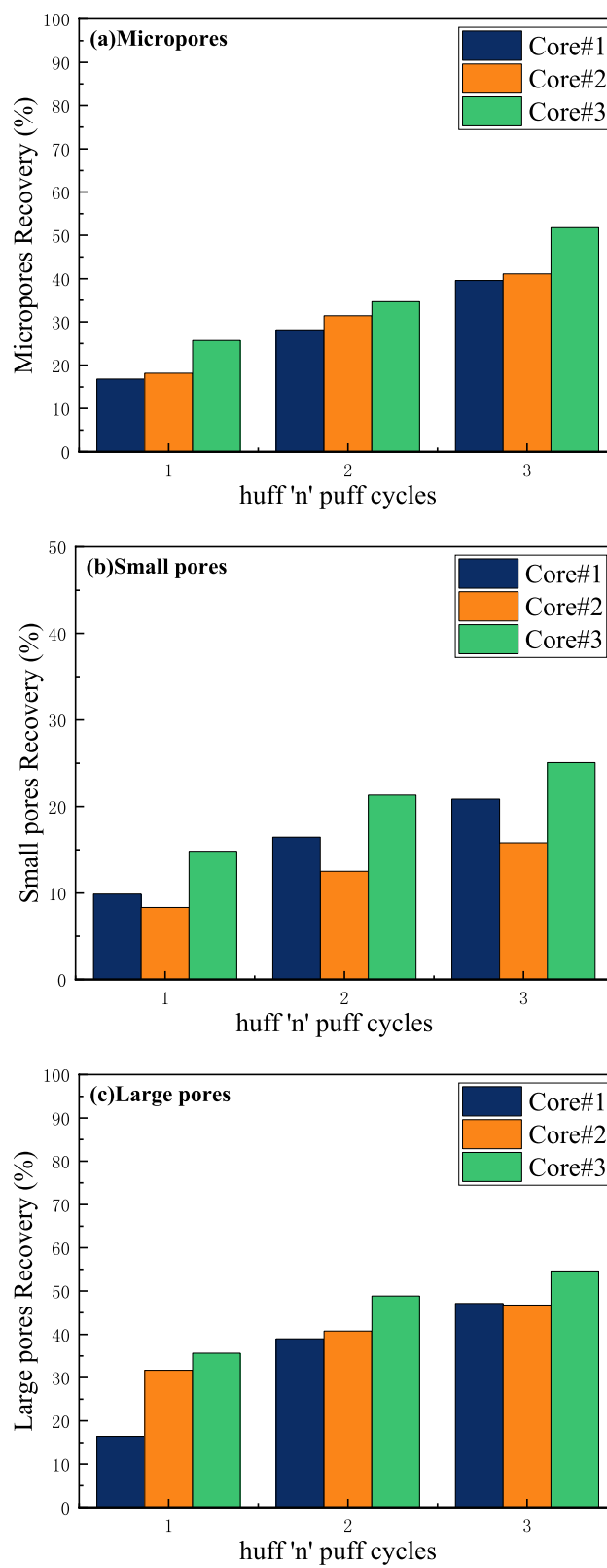


Fig. 7 Oil-recovery profiles of CO₂ huff 'n' puff plotted against cycle numbers (time) in different pore intervals

evident that, as the number of cycles increases, the recovery degree of the large pores initially increases and then tends to flatten out, while the recovery degree of the small pores increases linearly. This indicates that CO₂ first mainly acts on the shale oil in the large pores of the matrix, while relatively little CO₂ enters the micro and small pores of the rock matrix. At the end of the third cycle, as shown in Fig. 7, the recovery degree of the large pores was 47.14%, 46.77%, and 54.65%, respectively, and the recovery degree of the matrix large pores still dominated. This result suggests that CO₂ huff 'n' puff first utilizes the shale oil in the large pores, and then gradually utilizes the shale oil in the small pores. As the permeability of the core increases, the recovery degree in each pore interval also increases, especially for the results of the first cycle. Permeability is influenced by factors such as pore structure and tortuosity. The lower the permeability, the greater the diffusion resistance, the longer the diffusion path, and the easier it is for gas molecules to collide with and adsorb on pore walls, leading to momentum loss and hindered gas diffusion. Additionally, the lower the permeability of the core, the more significant the impact of permeability on diffusion.

3.4 Analysis of shale oil recovery degree in different pore intervals

The permeability of the matrix primarily affects the recovery degree during the first cycle of CO₂ huff 'n' puff, with a focus on the large pore intervals ($10 \text{ ms} < T_2 < 100 \text{ ms}$), which was increased from 16.42% to 36.64%. During the first cycle of CO₂ huff 'n' puff, a higher matrix permeability leads to a more efficient diffusion of CO₂ within a limited time. As the matrix permeability increases, the diffusion resistance of CO₂ decreases (such as diffusion distance, collision energy loss between molecules and walls, etc.). Allowing more CO₂ molecules to penetrate the shale matrix. This results in better expansion and recovery of shale oil. As the injection cycles progress, the diffusion time for CO₂ increases, and the differences in recovery between different matrix permeability levels diminish, although the high-permeability group (Core #3, 0.466 mD) still exhibits the highest recovery. As shown in Fig. 7, the increase in recovery is most significant in the large pore intervals within different scale pore intervals. This also indicates that CO₂ injection primarily mobilizes shale oil from the large pores, which is consistent with the findings of previous studies and Wei (2019).

4 Discussion and conclusions

In unconventional reservoirs, the mechanisms of enhanced oil recovery (EOR) methods significantly differ from those in conventional reservoirs due to their exceptional

petrophysical properties. Although previous studies have investigated the effects of exposing shale matrix to carbon dioxide (CO₂) for CO₂-EOR (Wei et al. 2019; Wang et al. 2017), only a few of them have experimentally considered the influence of different matrix permeability and the resulting effects on the transport of fluids within varying-scale pores between the matrix and fractures. This limitation is largely attributed to the currently available monitoring tools for shale formations.

In an effort to enhance our understanding of the CO₂-EOR mass transfer mechanisms in fractured shale reservoirs, we conducted an experimental investigation involving cyclic injection of CO₂ in three shale matrices (with the permeability of 0.074 mD/0.170 mD/0.466 mD) and fracture model under reservoir conditions. The core samples used in the study were obtained from the Lucaogou Formation. To gain insight into the pore-scale mobilization process, we monitored the entire process using a low-field NMR technique. Based on our findings, we draw the following general conclusions:

- (1) Observations under three different permeability conditions (0.074 mD/0.170 mD/0.466 mD) consistently demonstrate that CO₂ injection primarily recovers oil from large pores ($10 \text{ ms} < T_2 < 100 \text{ ms}$), while oil in small pores ($1 \text{ ms} < T_2 < 10 \text{ ms}$) and micropores ($0.1 \text{ ms} < T_2 < 1 \text{ ms}$) exhibits limited mobility.
- (2) After three cycles of CO₂ huff 'n' puff, the total recovery degree increased from 30.28% to 34.95% as the matrix permeability of the core samples increased from 0.074 to 0.466 mD, indicating a positive correlation between CO₂ extraction efficiency and matrix permeability. Under similar fracture conditions, the increase in matrix permeability can further promote CO₂ extraction efficiency during CO₂ injection.
- (3) The increase in matrix permeability of the core has the greatest effect on the extraction of the first-cycle injection in large pores, which was increased from 16.42% to 36.64%. As the matrix permeability increases, the diffusion resistance of CO₂ decreases (such as diffusion distance, collision energy loss between molecules and walls).

5 Research highlights

- (1) Positive correlation between matrix permeability and CO₂ extraction efficiency: The study found that the increase in matrix permeability from 0.074 to 0.466 mD resulted in an increase in total recovery degree from 30.28% to 34.95% after three cycles of CO₂ huff 'n' Puff.

- (2) Experimental investigation of mass-exchange behaviors: The research employed a LF-NMR technique to monitor the oil concentration in both matrix and fractures.
- (3) Insights into CO₂-enhanced oil recovery mechanisms: The research provides valuable complementary information on the effects of CO₂ huff 'n' Puff in different pore sizes following fracturing under varying permeability conditions.

Acknowledgements The authors would like to acknowledge the financial support from the National Natural Science Foundation of China via grant number 52174035, 52304048. This work is also supported by the China Postdoctoral Science Foundation (2022M722637) and Research and Innovation Fund for Graduate Students of Southwest Petroleum University (2022KYCX026).

Author contributions TX: Conceptualization, methodology, writing original draft. JW: Supervision, project administration, funding acquisition. YL: Formal analysis. DW: Visualization. LY: Validation. YT: Writing review and editing, funding acquisition.

Availability of data and materials Data available on request from the authors.

Declarations

Competing interests We declare that we have no financial and personal relationships with other people or organizations that can inappropriately influence our work, there is no professional or other personal interest of any nature or kind in any product, service and/or company that could be construed as influencing the position presented in, or the review of, the manuscript entitled.

Open Access This article is licensed under a Creative Commons Attribution 4.0 International License, which permits use, sharing, adaptation, distribution and reproduction in any medium or format, as long as you give appropriate credit to the original author(s) and the source, provide a link to the Creative Commons licence, and indicate if changes were made. The images or other third party material in this article are included in the article's Creative Commons licence, unless indicated otherwise in a credit line to the material. If material is not included in the article's Creative Commons licence and your intended use is not permitted by statutory regulation or exceeds the permitted use, you will need to obtain permission directly from the copyright holder. To view a copy of this licence, visit <http://creativecommons.org/licenses/by/4.0/>.

References

Al-Yaseri AZ et al (2015) Pore-scale analysis of formation damage in Bentheimer sandstone with in-situ NMR and micro-computed tomography experiments. *J Pet Sci Eng* 129:48–57

Amer MW, Aljariri Alhesan JS, Ghassan ALB (2022) Ultrasonic extraction of oil shale bitumen and study of its structural features using GC–MS and NMR techniques. *Int J Coal Prep Util* 43:1524–1541

Bardenhagen I, Dreher W, Fenske D, Wittstock A, Baeumer M (2014) Fluid distribution and pore wettability of monolithic carbon xerogels measured by H-1 NMR relaxation. *Carbon* 68:542–552

Burrows LC, Zitha PLJ, Masalmeh SK (2020) A literature review of CO₂, natural gas, and water-based fluids for enhanced oil recovery in unconventional reservoirs. *Energy Fuels* 34(5):5331–5380. <https://doi.org/10.1021/acs.energyfuels.0c00332>

Chaturvedi KR, Sharma T (2022) Modified smart water flooding for promoting carbon dioxide utilization in shale enriched heterogeneous sandstone under surface conditions for oil recovery and storage prospects. *Environ Sci Pollut Res* 29(27):41788–41803

Chi L, Heidari Z (2015) Diffusional coupling between microfractures and pore structure and its impact on nuclear magnetic resonance measurements in multiple-porosity systems. *Geophysics* 80(1):D31–D42

De Boever E et al (2016) Multiscale approach to (micro)porosity quantification in continental spring carbonate facies: case study from the Cakmak quarry (Denizli, Turkey). *Geochem Geophys Geosyst* 17(7):2922–2939

Enab K, Emami-Meybodi H (2021) Effects of diffusion, adsorption, and hysteresis on huff-n-puff performance in ultratight reservoirs with different fluid types and injection gases. *Energies* 14(21):6708. <https://doi.org/10.3390/en14216708>

Hu K, Zhang Q, Liu Y, Thaik AM (2023) A developed dual-site Langmuir model to represent the high-pressure methane adsorption and thermodynamic parameters in shale. *Int J Coal Sci Technol* 10(1):59. <https://doi.org/10.1007/s40789-023-00629-x>

Li X, Wei W, Xia Y, Wang L, Cai J (2023) Modeling and petrophysical properties of digital rock models with various pore structure types: An improved workflow. *Int J Coal Sci Technol* 10(1):61. <https://doi.org/10.1007/s40789-023-00627-z>

Liu X et al (2020) Pore structure petrophysical characterization of the upper cretaceous oil shale from the Songliao basin (NE China) using low-field NMR. *J Spectrosc* 2020:9067684

Liu W, Wang G, Han DY, Xu H, Chu XY (2021) Accurate characterization of coal pore and fissure structure based on CT 3D reconstruction and NMR. *J Nat Gas Sci Eng* 96:104242

Liu B, Yao J, Sun T (2023) Numerical analysis of water-alternating-CO₂ flooding for CO₂-EOR and storage projects in residual oil zones. *Int J Coal Sci Technol* 10(1):73. <https://doi.org/10.1007/s40789-023-00647-9>

Mahzari P, Abass H, Dusseault MB, Kantzas A (2021) Novel laboratory investigation of huff-n-puff gas injection for shale oils under realistic reservoir conditions. *Fuel* 284:119129. <https://doi.org/10.1016/j.fuel.2020.119129>

Menefee AH, Ellis BR (2020) Regional-scale greenhouse gas utilization strategies for enhanced shale oil recovery and carbon management. *Energy Fuels* 34(5):6136–6147

Saeed SA et al (2022) Hydrothermal conversion of oil shale: synthetic oil generation and micro-scale pore structure change. *Fuel* 312:122786

Sharma S, Agrawal V, Akondi RN (2020) Role of biogeochemistry in efficient shale oil and gas production. *Fuel* 259:116247. <https://doi.org/10.1016/j.fuel.2019.116247>

Shen R et al (2022) Study on fluid mobility in sandwich-type shale oil reservoir using two-dimensional nuclear magnetic resonance approaches. *Energy Sources Part A Recov Util Environ Eff* 44(3):5951–5967

Su Y, Sun Q, Wang W, Guo X, Xu J, Li G, Shi Z (2022) Spontaneous imbibition characteristics of shale oil reservoir under the influence of osmosis. *Int J Coal Sci Technol* 9(1):69. <https://doi.org/10.1007/s40789-022-00546-5>

Taheri-Shakib J, Kantzas A (2021) A comprehensive review of microwave application on the oil shale: prospects for shale oil production. *Fuel* 305:121132. <https://doi.org/10.1016/j.fuel.2021.121132>

- Tan X, Zhang J, Wang Y, Li M, Liu J, Zhu Z (2023) Application of a salt-resistant in situ cross-linked terpolymer gel for the Daqing Oilfield. *ACS Omega*. <https://doi.org/10.1021/acsomega.3c02446>
- Wang H, Lun Z, Lv C, Lang D, Pan W, Luo M, Chen S (2017) Nuclear-magnetic-resonance study on mechanisms of oil mobilization in tight sandstone reservoir exposed to carbon dioxide. *SPE J* 23(03):750–761. <https://doi.org/10.2118/179554-PA>
- Wang H, Lun Z, Lv C, Lang D, Luo M, Zhao Q, Zhao C (2020) Nuclear-magnetic-resonance study on oil mobilization in shale exposed to CO₂. *SPE J* 25(1):432–439
- Wei B et al (2020) Nuclear-magnetic-resonance monitoring of mass exchange in a low-permeability matrix/fracture model during CO₂ cyclic injection: a mechanistic study. *SPE J* 25(1):440–450
- Xu T, Wang J, Lyu W, Zhang Y, Lu Y (2022) Experimental study of diffusion and formation mineral change in supercritical CO₂ huff and puff process of shale reservoir. *Lithosphere* 2022(Special 12):6171981. <https://doi.org/10.2113/2022/6171981>
- Yang P, Guo H, Yang D (2013) Determination of residual oil distribution during waterflooding in tight oil formations with NMR relaxation measurements. *Energy Fuels* 27(10):5750–5756. <https://doi.org/10.1021/ef400631h>
- Zhao J, Yang L, Yang D, Kang Z, Wang L (2022) Study on pore and fracture evolution characteristics of oil shale pyrolysed by high-temperature water vapour. *Oil Shale* 39(1):79–95